Review Article

What can biophotonics tell us about the 3D microstructure of articular cartilage?

Stephen J. Matcher[1,2]

[1]Department of Materials Science and Engineering, [2]INSIGNEO Institute for in-silico medicine, University of Sheffield, North Campus, Broad Lane, Sheffield, S3 7HQ, UK

Correspondence to: Stephen J. Matcher. Department of Materials Science and Engineering, University of Sheffield, North Campus, Broad Lane, Sheffield, S3 7HQ, UK. Email: s.j.matcher@sheffield.ac.uk.

Abstract: Connective tissues such as articular cartilage have been the subject of study using novel optical techniques almost since the invention of polarized light microscopy (PLM). Early studies of polarized light micrographs were the main evidential basis for the establishment of quantitative models of articular cartilage collagen structure by Benninghoff and others. Even now, state of the art optical techniques including quantitative polarized light microscopy (qPLM), optical coherence tomography (OCT), polarization-sensitive optical coherence tomography (PS-OCT), second harmonic generation (SHG) microscopy, Fourier-transform infrared (FTIR) microscopy, Raman and optical hyperspectral reflectance and fluorescence imaging are providing new insights into articular cartilage structure from the nanoscale through to the mesoscale. New insights are promised by emerging modalities such as optical elastography. This short review highlights some key recent results from modern optical techniques.

Keywords: Articular cartilage; collagen; birefringence; polarized light microscopy (PLM); optical coherence tomography (OCT); multi-photon microscopy; vibrational spectroscopy; multi-spectral microscopy

Submitted Nov 27, 2014. Accepted for publication Dec 02, 2014.
doi: 10.3978/j.issn.2223-4292.2014.12.03
View this article at: http://dx.doi.org/10.3978/j.issn.2223-4292.2014.12.03

Introduction

Optical and infrared techniques have played, and continue to play, a major role in monitoring many aspects of cartilage. Cartilage derives its unique mechanical properties through an interaction between the 3-D architecture of the collagen matrix and the osmotic pressure generated by interstitial water and proteoglycans. Articular cartilage plays a vital role in providing a low-friction surface between the bones of articulating joints (1). Cartilage degeneration due to non-inflammatory processes (trauma, age) is collectively termed "osteoarthritis" and is a leading cause of disability in the western world. Left untreated it progresses to complete cartilage destruction and hence intense pain due to bone-on-bone friction. The only viable treatment is then a total joint replacement. In the elderly these can be very effective however in those under 40 there is a major problem of limited implant lifetime, due to effects such as aseptic loosening. Hence there is considerable interest in early diagnosis and in developing and monitoring restorative cartilage treatments (2). There are several areas in which optical techniques can be of benefit.

Polarized light microscopy (PLM)

Optical birefringence has been a known property of articular cartilage since the early 19th century (3). PLM refers to the general technique of imaging histological sections using polarized illumination and detection, historically and most commonly by placing the section between crossed polarizers. A cartilage section has a distinctive appearance between crossed polarizers. For the correct orientation it is found that the superficial and deep layers appear bright whereas the intervening layer appears dark. This is generally interpreted as strong optical birefringence in

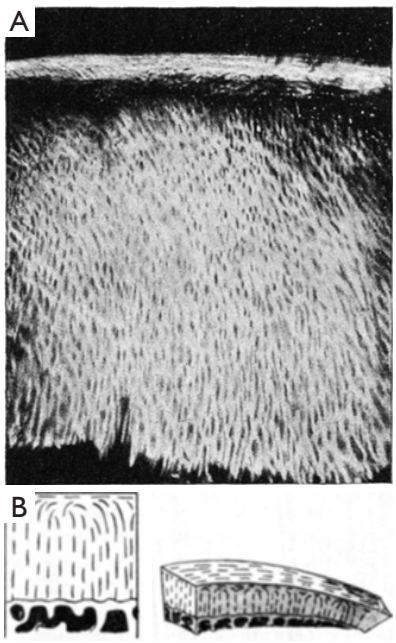

Figure 1 Benninghoff's original micrographs and sketches of his proposed "arcade" model of collagen fiber organization in articular cartilage. (A) The 40 m section of human patella cartilage transilluminated between crossed Nicol prisms, whose transmission/extinction axes are at 45° to the tangential layer. The section is cut parallel to the superficial "split-line". Note the strong signal in the tangential and radial zones and the weak signal in between these. Reproduced from Benninghoff (4) with permission. (B) Benninghoff's proposed cartilage architecture.

the superficial and deep layers and weaker birefringence in the intermediate layer. Considerations of this type led Benninghoff to propose his now famous "arcade" model of collagen organization (*Figure 1*). In this model the collagen fibers are oriented normally to the joint surface where they anchor to the cartilage-bone interface, then curve as they approach the surface, to run parallel to the surface at the uppermost extent before then arching back over the descending back towards the cartilage/bone interface and reattaching at an orientation normal to the surface (4).

Hence individual fibers were considered to form a continuous "gothic arch" structure. More recently, by combining the polarized-light measurements with cryofracture SEM images, this model has been revised somewhat to one in which the collagen fibers form a stack of parallel lamellae, i.e., a "leaf" structure, in which the leaves arch over to become parallel with the cartilage surface (5,6). Based on such observations, cartilage is generally considered to comprise three distinct layers, the radial layer adjacent to the bone-cartilage interface and containing vertically aligned fibers, the superficial (a.k.a tangential) layer, within 100-200 μm of the surface wherein the fibers run parallel to the surface and in between these layers a "transitional" zone. Generally this zone appears darker than the other two zones under PLM. The low birefringence in the transitional zone is generally attributed to a more disordered fibrillar microstructure in that zone.

Historically PLM has been a semi-quantitative technique because a single observation made through crossed-polarizers is not sufficient to fully characterize the optical anisotropy of a material. The combination of polarization-controlling elements such as liquid crystal retarders, coupled with digital cameras and computer processing has led to the development of quantitative polarized light microscopy (qPLM). Rieppo recently reviewed this generic approach and described a system using motorized rotating crossed polarizers and a quarter-wave plate which can automatically determine the absolute birefringence and collagen fibril orientation (actually the optical "slow-axis") on a pixel-by-pixel basis (7). They termed this technique "enhanced polarized light microscopy" or ePLM. These microscopes operate in the transmission mode on thin histological slices. They can produce 2-D maps of birefringence and slow-axis orientation with 10-50 μm spatial resolution. An additional parameter can be extracted from ePLM data, which Rieppo *et al*. term the "parallelism index" or PI. This index is generally defined via the ratio of the maximum to minimum light transmission through the sample as a function of polarizer orientation and has been suggested to be an indicator of local fibrillar directional order. Of course, linear birefringence is also affected by fibrillar organization (being zero for a state of isotropic 3-D fibrillar orientation) and so the relationship between these parameters deserves detailed investigation.

Xia *et al*. introduced the qPLM technique into the systematic study of cartilage in 2001 (8). Quantitative maps of both birefringence and slow-axis orientation were produced for a sagittal slice through canine humeral head cartilage tissue (*Figure 2*). The transitional zone was identified by a rapid change in slow-axis orientation from 90° to zero and associated with this was a dip in birefringence, consistent with a zone of disorganized cartilage. The birefringence did not vanish completely in the transitional zone however, which the authors interpret as showing that cartilage retains a degree of order throughout all regions. More recently Mittelstaedt *et al*. have used qPLM but applied to transverse rather than sagittal sections of canine humeral head cartilage (9). An

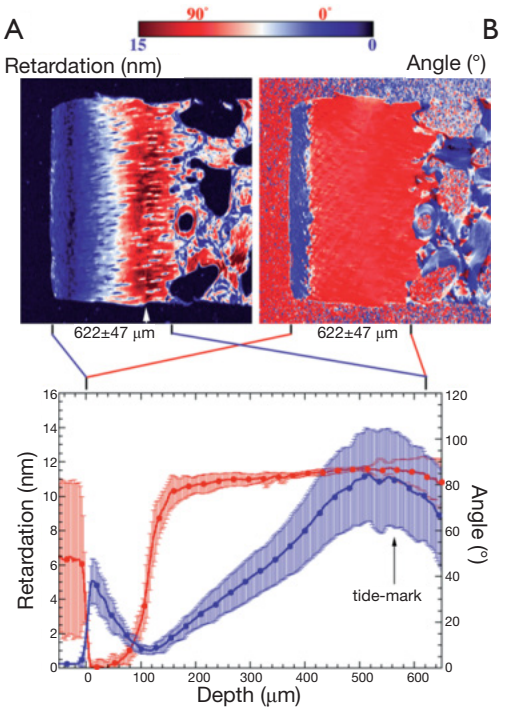

Figure 2 Cartilage section analysed using the qPLM technique. The true retardance and fast-axis orientation are determined by this extended polarized light technique. Reproduced from Xia *et al.* (8) with permission. A clear minimum in the retardance at ~120 m depth is interpreted as the disorganized collagen of the "transitional zone". qPLM, quantitative polarized light microscopy.

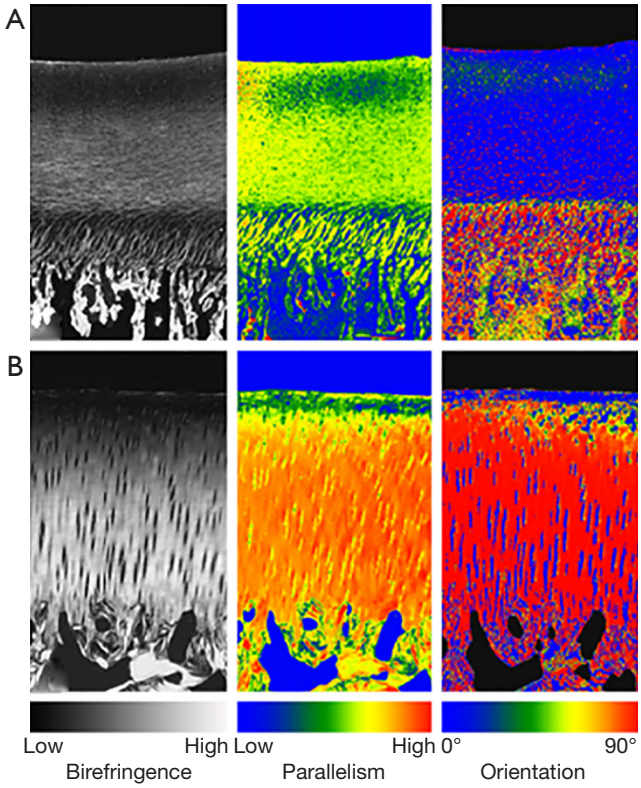

Figure 3 qPLM images of porcine femoral trochlea cartilage at 4 months maturation (A) and 21 months maturation (B). A classic "Benninghoff" type architecture with a thick radial zone and thin superficial zone is only observed in the older animal. At 4 months the whole cartilage thickness is dominated by a superficial zone. Reproduced from Rieppo *et al.* (10) with permission. qPLM, quantitative polarized light microscopy.

interesting observation is that the azimuthal angle of the dominant collagen alignment direction is not constant with depth, as it would be, e.g., with tendon. Instead the optical "slow-axis" rotates through up to 40 degrees of azimuth between the surface and 500 microns depth.

Rieppo *et al.* used ePLM to study maturational changes in porcine femoral groove articular cartilage from animals of ages 4, 11 and 21 months (10). Substantial changes were found in the birefringence, fiber orientation and parallelism index as functions of age (*Figure 3*). It was found that the Benninghof architecture develops along with skeletal maturity and has not developed at all in 4-month-old pigs (human equivalent age ~6-8 years). Instead the immature animals appear to possess a cartilage collagen architecture that is dominated by the superficial layer, so that the dominant fiber alignment direction is parallel with the surface. By 21 months (human age equivalent 20-25 years) the Benninghoff architecture has appeared and, in addition, the total birefringence in the radial zone increases substantially. The authors interpret these findings as indicating that collagen remodelling in response to increased muscle strength and joint loading is ongoing before skeletal maturity is reached, eventually falling due to decreased collagen synthesis and decreased levels of matrix metalloproteinases.

The quantitative data produced by these systems can find a practical use in cartilage biomechanical modelling. One of the post popular materials models for cartilage at the present time is the fibril-reinforced porous visco-elastic model (FRPVE) model, e.g., (11). This biphasic model considers that the mechanical properties arise principally from a fluid phase (interstitial water) and a solid phase (collagen fibrils and proteoglycans). The collagen fibrils are primarily believed to determine the tensile stiffness and dynamic compressive stiffness hence these models specify the depth-dependent collagen orientation. Julkunen *et al.* combined information

from qPLM, such as the thickness of the superficial zone and the fiber bending radius, into the FRPVE model, allowing a more accurate prediction of depth-dependent compressive stresses and strains than previous models based on homogeneous fibril distributions (12).

An interesting finding from combined MRI T2 mapping and qPLM is the appearance of a second zone of tangentially oriented collagen fibers, midway between the surface and the bone-cartilage interface, in juvenile bovine patellar cartilage (13).

Optical coherence tomography (OCT)

Whilst qPLM is a very powerful photonics tool for structural characterization, by nature it can only be applied *ex vivo* because of the need to transmit light through a histological section. The advent of non-invasive optical modalities such as confocal microscopy and OCT bring the possibility to gain information *in vivo*, by supplementing a conventional arthroscopy examination. Photonics can thus move from characterization to diagnosis.

OCT is a volumetric imaging tool similar conceptually to ultrasound (US) but using light rather than acoustic waves. It is distinguished from US by (I) 2-10 micron depth resolution compared with typically 100-1,000 micron depth resolution for clinical US; and (II) 1-2 mm imaging depth *vs*. 10-100 mm imaging depth for clinical US. It is thus ideal for imaging the surface layers of accessible tissues (endothelium, retina, articular cartilage). The penetration depth is sufficient to image through to the cartilage-bone interface for small human joints and to image the superficial regions of thicker cartilage such as in the human knee.

The earliest report on OCT of cartilage was by Herrmann *et al*. at MIT (14). The study examined OCT images taken *ex vivo* on excised human specimens. In total over 100 samples from 10 subjects were taken, covering knee, hip, interphalangeal, metatarsal, intervertebral, elbow, clavicular and ankle. OCT imaging with 5 micron axial resolution provided much greater information than other non-destructive modalities such as radiography or MRI, albeit with the need to physically penetrate into the joint-space in the same way as visible arthroscopy. Fibrosis, presumably due to fibrocartilage repair tissue, and surface fibrillations were readily detected. In addition, polarization sensitivity was detected from the highly organized collagen in the interphalangeal joint of the second toe. This was quantified in a comparatively simple way, namely by modulating the polarization state of the incident light and comparing the appearance of the OCT image. The authors speculated on the potential early diagnostic value of such measurements, as disruptions of collagen organization are believed to be an early marker for osteoarthritic degeneration. OCT imaging can be developed into a tool that quantitatively determines birefringence, similar to qPLM but non-destructively, and this has led to further insights (see next section).

Chu *et al*. evaluated clinical arthroscopic OCT imaging as a means to improve the detection of surface fibrillation and internal defects such as splits and fissures (15). Using a rigid arthroscope beam delivery system they obtained cross-sectional B-scan images in-situ from donated human cadaver knees and also from *ex vivo* osteochondral cores harvested from osteoarthritic human tibial plateaus (*Figure 4*). The authors found that the rigid arthroscope OCT system could readily image the medial and lateral femoral condyle and trochlea on the intact joint, however, the tibial plateau was not accessible because of the distal probe orientation. A comparison against conventional arthroscopy and histology showed that OCT matched histology in its ability to detect subtle surface fibrillation in areas that appeared to be free of damage by arthroscopy. This suggests a potential role for arthroscopic OCT in guiding debridement treatments, where real-time feedback to the surgeon would be beneficial in selecting suitable treatments sites and monitoring the progress of the treatment.

Recently the use of a completely flexible probe, designed originally for intravascular OCT imaging, has also been demonstrated (16). The 0.9 mm diameter flexible probe in this system enabled OCT imaging within the intact first carpometacarpal joint of a human cadaver. Cartilage thicknesses of 0.6 and 1.1 mm were directly measured. Evidence of surface fibrillation and fissuring was detected. This same probe was used in a similar study on the equine metacarpophalangeal joint (17). High quality images were obtained by inserting a Dragonfly intravascular OCT catheter (St Jude Medical) through a dorsomedial portal, whilst a standard arthroscope was inserted through a standard portal. A direct comparison between the two modalities confirmed OCT's better sensitivity at detecting surface fibrillation and fissuring and its ability to detect subsurface lesions. The relative thinness of equine cartilage at this site also allowed direct measurement of the cartilage thickness. OCT allowed a less subjective scoring of cartilage lesions and could be beneficial in selecting the most appropriate treatment and monitoring treatment response.

In small animals such as rodents, OCT imaging can measure the cartilage thickness directly, and this has been

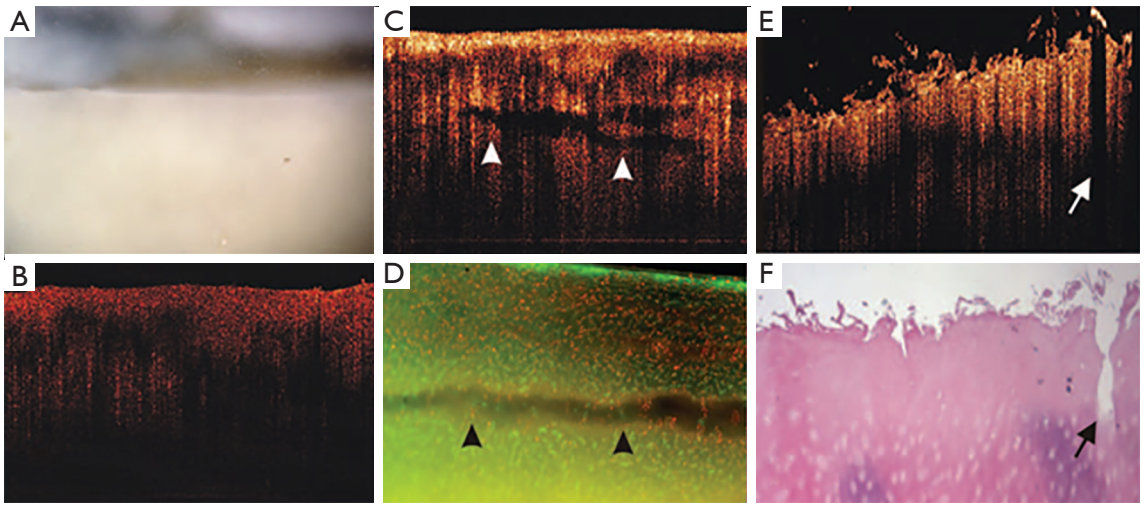

Figure 4 Arthroscopic OCT imaging of human knee cartilage samples that display chondromalacia, uniformly graded 0/1 by conventional surface imaging. OCT is able to provide additional discrimination between these samples, with image B revealing an intact surface whilst C shows subsurface clefts and E shows fissures and fibrillations. Reproduced from Chu *et al.* (15) with permission. OCT, optical coherence tomography.

used to demonstrate thinning in response to drug-induced osteoarthritis. By injecting the knee joints of Wistar rats with sodium iodoacetate and then imaging with OCT at 1,300 nm wavelength, Patel *et al.* demonstrated a consistent drop in cartilage thickness and disruption of the bone-cartilage interface (18). By modulating the polarization state of the incident light and observing any changes in the OCT image, it was also concluded that the drug-induced osteoarthritis effectively eliminated the birefringence of the tissue, presumably by destroying the strong directional alignment of the collagen fibers.

It has also been found that OCT can infer optical properties, such as the near-infrared backscatter and extinction coefficients (19), and that a change in these correlates with degeneration and also with impact loadings. Bear *et al.* compared the OCT signal intensity ratio between superficial and radial zones in *ex vivo* bovine tibial plateau cartilage, both before and 12 hours after impacts of low energy (0.175 J) and moderate energy (0.35 J) created by dropping a weighted indenter onto the surface (20). Impact injury consistently raised the surface signal intensity and decreased the deep signal intensity, suggesting an increase in backscatter and attenuation coefficients. Histology showed an increase in chondrocyte death and surface collagen matrix disruption, which together may account for the changes in optical properties.

A more quantitative characterization of cartilage optical properties by OCT was reported by Shyu *et al.* (21). By measuring the full profile of OCT image brightness versus depth a quantitative comparison could be made against a theoretical model based on the extended Huygens-Fresnel principle (22). Using cartilage samples from a "porcine joint", the authors identified areas appearing visibly normal and showing visible minor damage. The OCT brightness *vs.* depth was then fitted using an analytical model which includes, as its free parameters, the attenuation coefficient and the "effective anisotropy factor" (which describes the angular dependence of light scattering). Damaged cartilage showed a tendency to produce larger attenuation coefficients than normal cartilage and there was also a tendency for damaged cartilage to produce more isotropic scattering.

Polarization-sensitive (PS) OCT

Unlike ultrasound in soft tissue, light waves are transverse and can thus carry polarimetric information. Combining polarimetry with OCT leads to a new technique called PS-OCT (23). PS-OCT can detect areas of enhanced or reduced birefringence in cartilage. Enhanced birefringence can be associated with a repair mechanism, in which degenerated hyaline cartilage (chiefly composed of type-II collagen) is replaced by fibrocartilage (predominantly type-I collagen). The fibrocartilage often has thickened, denser fibers which appear bright on a structural OCT image.

Li *et al.* used a polarized light structural OCT imaging system to study human knee joints *in vivo* prior to partial

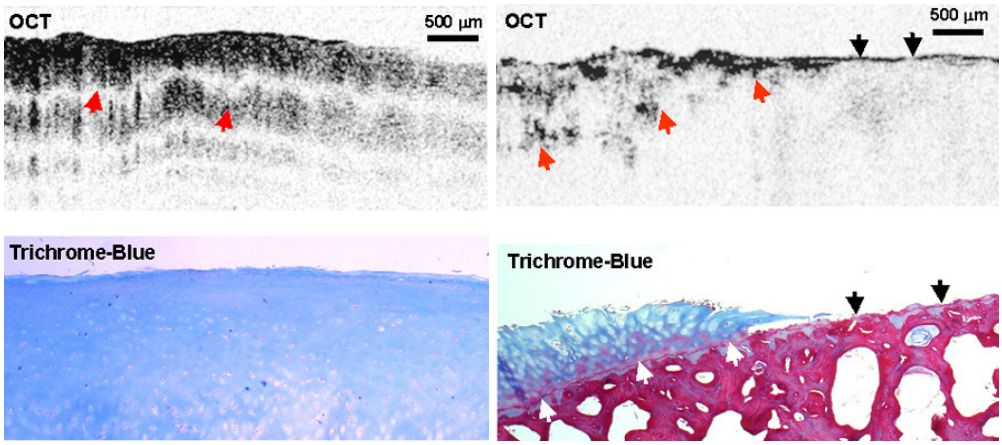

Figure 5 *In vivo* polarization-sensitive OCT imaging of human knee cartilage, taken during knee replacement surgery. Upper row shows PS-OCT images, lower row shows contemporary histology, with Masson trichrome staining for collagen. Normal knee cartilage displays a uniform pattern of banding, suggesting a thick layer of organized birefringent collagen fibers. Exposed bone lacks obvious banding, as does degraded cartilage in the vicinity of the lesion. Reproduced from Li *et al.* (24) with permission. OCT, optical coherence tomography; PS-OCT, polarization-sensitive optical coherence tomography.

or total joint replacement treatment (24). The excised cartilage was then examined histologically using Trichrome-blue staining and registered with the PS-OCT images (*Figure 5*). Visibly normal human knee cartilage showed a regular depth-resolved banding pattern, caused by the modulation of the incident polarization state of the light due to birefringence from the organized collagen in the cartilage. This banding pattern was consistently lost in cartilage showing advanced degeneration by Trichrome-blue staining.

Chu *et al.* investigated the use of PS-OCT birefringence to grade femoral condyle and trochlea osteoarthritic lesions in human cadaver knees (25). PS-OCT (implemented using a polarized light structural OCT system) identified *ex vivo* cartilage samples displaying pronounced birefringence and also samples displaying no obvious birefringence. Whilst the latter observation would most naturally be interpreted as a complete loss of collagen organization, the authors found that this loss of birefringence was potentially a marker of very early stage loss of chondrocyte viability. By measuring proteoglycan synthesis before and after stimulation with IGF-1 growth factor, it was found that cartilage that lacked birefringence had lost its ability to respond to IGF-1 by upregulating proteoglycan production. Interestingly however, this loss of IGF-1 sensitivity appeared to be reversible by administering L-NMA to block nitric oxide synthase. Hence the absence of form birefringence might conceivably be an indicator for early stage degeneration at a point where it could still be reversed pharmacologically.

Recently our lab introduced two related variants of PS-OCT, which we have termed variable-incidence-angle PS-OCT (VIA-PS-OCT) (26-28) and conical-scan PS-OCT (CS-PS-OCT) (29). These two methods are specifically targeted at quantifying the 3-D zonal architecture of cartilage collagen by modifying the incidence angle of the light beam relative to the collagen fibers. The methods exploit the fact that the apparent birefringence of a sample is determined not just by the abundance and directional organization of collagen but also by the orientation of the collagen fiber long axis relative to the direction of the incident light beam (30,31). The apparent birefringence vanishes when these two directions are parallel (or anti-parallel) and reaches a maximum when they are orthogonal. CS-PS-OCT varies the relative orientation by sweeping the incident beam around the surface of a cone, whose tip lies at the tissue surface. A conical-scan of depth-resolved retardance often displays a highly anisotropic pattern which we have termed the "comet-crescent": the crescent-shaped retardance band and the extended "comet-tail" imply a directional anisotropy to the macroscopic collagen organization which can be explained by reference to the cryo-SEM studies of Clark (5) and of Jeffery *et al.* (6).

Our data also implies that the collagen fibers are "brushed" in a particular direction, such that at one particular point on the cone, the incident light beam is very close to being parallel to the fibers, whereas a further

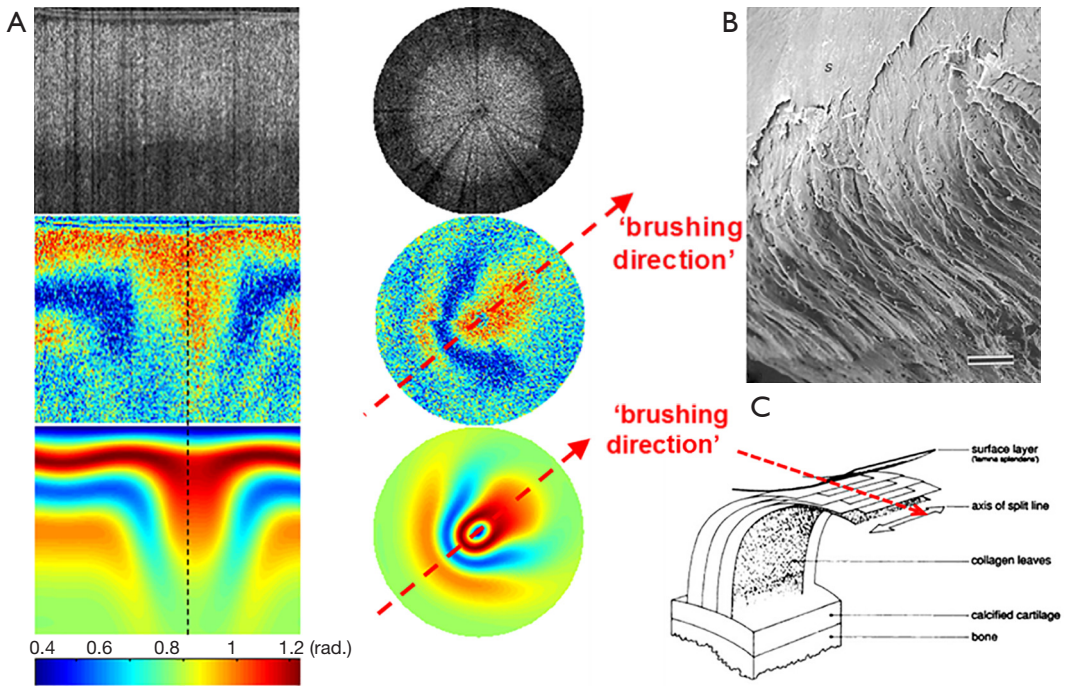

Figure 6 (A) Conical scan OCT image of cartilage backscatter (upper row) and retardance (middle row), reproduced with permission from Lu *et al.* (29). (B) SEM image of the collagen microstructure in intact cartilage, implying a "leaf-like" arrangement of fibers. Reproduced with permission from Clarke (5). (C) Schematic of the leaf-like arrangement, showing the preferred direction referred to as the "brushing direction". Reproduced with permission from Jeffery *et al.* (6). (A) (bottom row): output from an analytical model of conical-scan PS-OCT. The extended "tail" points in the brushing direction. OCT, optical coherence tomography; PS-OCT, polarization-sensitive optical coherence tomography.

180 degrees of azimuth rotation brings the beam to a point where it is closer to being orthogonal. The comet-tail represents a depth-resolved retardance profile of a very weakly birefringent medium and thus shows the direction in which the fibers have been brushed (*Figure 6*).

This observed "brushing direction" is a structural parameter of cartilage that has been little-studied in comparison to, say, the split-line direction. The split-line has been extensively mapped across a variety of species and sites. It is known from mechanical testing that cartilage from the superficial layer displays highly anisotropic mechanical properties, in particular it has been noted by a number of groups that cartilage has a markedly higher tensile Young modulus when loaded in a direction aligned with the split-line versus orthogonal to it. Based on this, Below *et al.* comprehensively mapped the split-line orientation across the distal human femur and hypothesized that osteochondral grafting might be more successful if the graft plug was oriented such that its split-line direction coincided with that at the defect site. The split-line is defined only over the angle range –90° to +90°, i.e., the split-line has a well-defined orientation but not a well-defined direction. The brushing direction however is uniquely defined over the full range –180° to +180°, which means that it represents a unique direction in space, i.e., there is a forward/backward anisotropy that is not revealed by the split-line. We speculate that the observed brushing direction might reflect the magnitude and direction of the dominant shear-stress that is experienced at that site during normal locomotion, i.e., the fibers are brushed flat in a particular direction at sites of high shear loading. It is thus interesting to speculate as to whether matching the brushing direction might provide benefits in osteochondral grafting also.

The pronounced variation in apparent birefringence with beam orientation is most clearly seen on cartilage samples taken from large animals. We first observed the effect in mature equine metacarpophalangeal cartilage (30) and our observation was confirmed by Xie *et al.* using cartilage taken from the femoral-tibial joints of 5- to 7-year-old bovines (31). An observation common to both groups

is that these samples frequently display very little apparent birefringence when imaged with a light beam that is applied at normal incidence to the tissue surface, which is the usual geometry for an OCT scan. The beam must be inclined by a substantial angle to reveal the underlying birefringence. On the other hand, workers who predominantly study human samples from, e.g., the knee usually report strong apparent birefringence for healthy cartilage tissue and a beam applied at normal incidence (24,25). A possible reconciliation of these observations is to note that low apparent birefringence at normal beam incidence is consistent with an imaging field that is dominated by the radial zone (fibers parallel to the beam direction) whereas high apparent birefringence suggests that the superficial zone (fibers orthogonal to the beam) dominates. Recalling the observations using ePLM of the collagen structure in skeletally maturing porcine knees (10), it may be that the much lower contact pressure in the human knee (lower body mass and larger contact area) compared with the equine and bovine joints favours a collagen architecture in which the superficial zone is physically much thicker. Techniques such as conical-scan PS-OCT may thus have a role in differentiating between a loss of birefringence due either to true disorganisation of the collagen fibers at the microstructural level or to a reduction in the superficial zone thickness, resulting from stress-induced remodelling or debridement.

Multi-photon microscopy and second harmonic generation imaging

When an ultrashort (~100 fs) pulse of light from a mode-locked laser irradiates tissue containing fluorophores then two-photon excitation can be used to obtain depth-resolved images of the fluorophore down to depth of several hundred microns, which is much greater than for one-photon fluorescence excitation. Whereas linear birefringence and one-photon absorption/fluorescence are mediated by the first order dielectric susceptibility tensor $\chi^{(1)}$, such two-photon processes are mediated by the second order nonlinear susceptibility tensor $\chi^{(2)}$. Yeh *et al.* used this effect to study articular cartilage, especially the superficial zone of the bovine femoral, tibial and patellar cartilage (32). They showed that the extracellular matrix of bovine articular cartilage produces both two photon fluorescence and second harmonic, if excited at wavelengths below 800 nm. Increasing the wavelength above this almost completely eliminates the fluorescence but not the SHG. They noted that the SHG from normal cartilage lacked a strong dependency on the polarization direction of the light beam but that fibrocartilage repair tissue produced much stronger polarization dependence. This is consistent with the greater content of aligned type-I collagen fibers that are expected in fibrous repair tissue and the earlier observations made using PS-OCT that fibrocartilage produces stronger linear birefringence than healthy hyaline cartilage.

Building on this work, our lab investigated SHG and TPEF from equine cartilage specimens (metacarpophalangeal joint) and found that normal hyaline cartilage displays polarization-sensitive SHG from the intact superficial zone (33). Since the collagen fibers were too small to visualize directly (unlike tendon) this provided an indirect means of measuring fiber alignment in the superficial zone. SHG images taken at regions far from a visible osteoarthritic lesion appeared smooth and inhomogeneous, with embedded chondrocytes appearing as dark voids (*Figure 7*). The chondrocytes display a bright pericellular rim under TPEF. At the site of the lesion, however, the SHG image becomes strongly fibrillated in structure, likely indicating the replacement of hyaline cartilage with fibrocartilage. The chondrocytes lose their bright nuclei and pericellular rims under TPEF, possibly indicating metabolic cell death. Interestingly, at regions approaching the lesion but still visually "normal", the SHG image appears noticeably different to that further from the lesion, with a much brighter pericellular rim appearing in the SHG channel. Observations of this type might one day lead to a label-free high resolution arthroscopic imaging tool, as SHG imaging can be performed endoscopically using double-clad photonic crystal fibers (34).

SHG emission from fibrillar tissues also displays strong polarization-dependence (35) and this can potentially be used to add some degree of chemical specificity to the technique, specifically by allowing the label-free discrimination of type-I and type-II collagen. Su *et al.* examined specimens of rat tail tendon (dominated by type-I collagen) and rat tracheal cartilage (dominated by type-II) using an SHG microscope in which the polarization orientation θ of the linearly polarized excitation light could be rotated and the unpolarized emission I detected (36). By comparing the resulting I(θ) with a theoretical curve it is possible to determine the ratio of three independent elements of the $\chi^{(2)}$ tensor: χ_{ZZZ}/χ_{ZXX} and χ_{XZX}/χ_{ZXX}. Histograms of these values collected for images of the two samples show consistent differences for the two collagen types (*Figure 8*). Since the measurements can be made without sectioning or labelling, such measurements could potentially be useful in diagnosis (fibrocartilage repair tissue is predominantly type-I collagen whereas natural

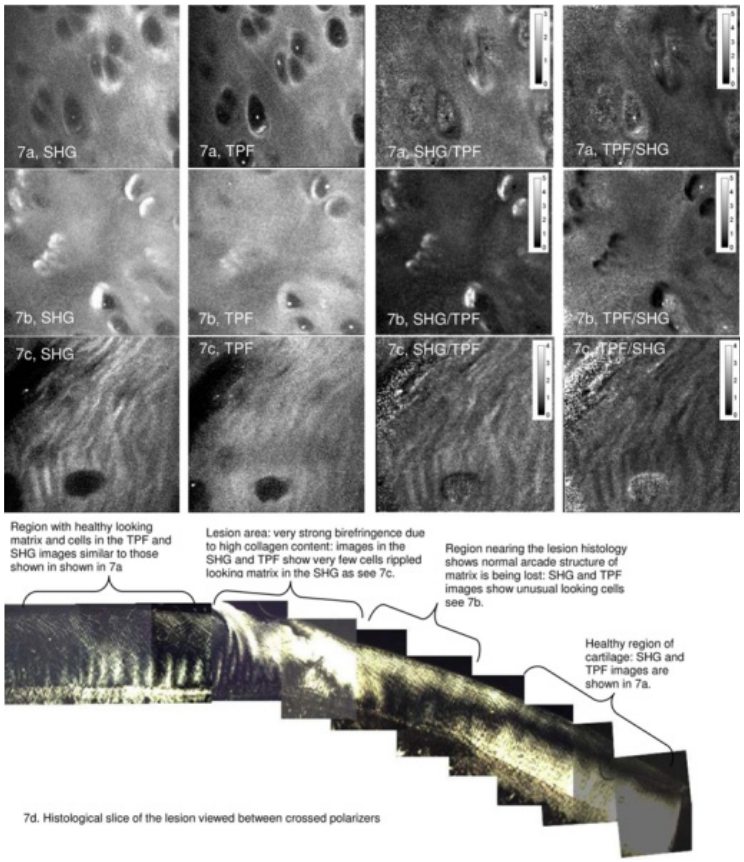

Figure 7 SHG and TPF images taken from three sites on the surface of an equine metacarpophalangeal sample displaying a visible osteoarthritic lesion. (A) SHG (column 1) and TPEF (column 2) from a site appearing visibly normal and far from the lesion, with polarized light imaging (bottom) showing an intact Benninghoff architecture. (B) A visibly normal site near the lesion, where polarized light imaging implies some loss to the arcade structure. SHG images show cells with an abnormally bright pericellular rim. (C) The site of the lesion, with polarized light imaging showing highly birefringent fibrous repair tissue. SHG images appear fibrillated and TPEF image lack cell nuclei. Reproduced from Mansfield *et al*. (33) with permission. SHG, second harmonic generation.

hyaline cartilage is mainly type-II) and in tissue engineering therapies (where hyaline repair cartilage is sought).

An interesting and essentially unanticipated observation from Yeh *et al*.'s seminal study was the detection of elastin fibers in the superficial zone. Elastin was detected and separated from collagen in an SHG/TPEF image due to its characteristic significantly longer peak two-photon excitation wavelength (~800 nm) and the presence of fibers whose directions were not correlated with the SHG signal from collagen (*Figure 9*). The observation was confirmed by Verhoeff staining. Yu and Urban developed this study further, using anatomical sectioning of the bovine metacarpophalangeal joint coupled with immuno-labelling using polyclonal rabbit anti-human alpha elastin (37). Conventional fluorescence micrographs, taken both in radial and transverse sections, then revealed a dense, ordered elastin network in the superficial zone of the cartilage but generally much sparser in deeper zones.

An interesting alternative application for high-resolution en-face imaging of cartilage is elastographic mechanical property measurement using digital image correlation techniques. Bell *et al.* used en-face two-photon imaging of excised cartilage samples taken from the equine metacarpophalangeal joint to track micron-scale displacement of chondrocytes in response to applied tensile stress (38). This allowed mapping of the "local strain deviation" (LSD) relative to the global strain at various positions on the cartilage surface and depths below it. Significant variations in local strain were detected, suggesting that variations in the anisotropy of the collagen network exist at the cellular scale.

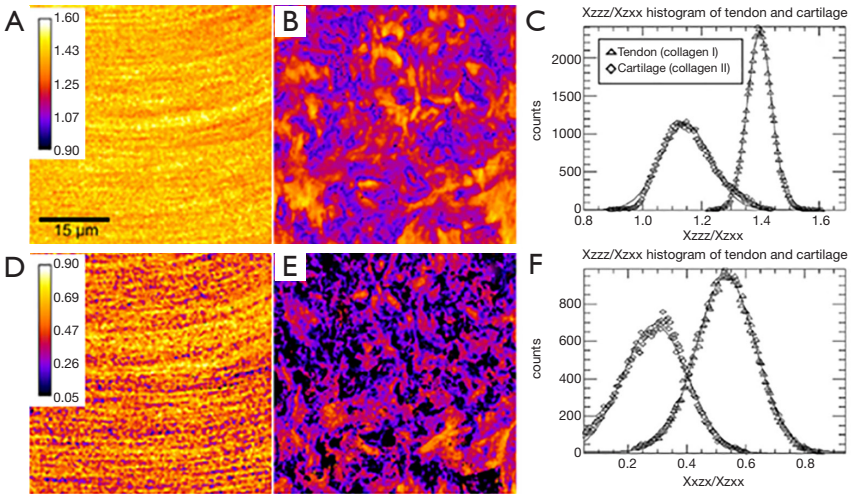

Figure 8 Histograms of the ZZZ/ZXX and XZX/ZXX ratios determined by polarization-resolved SHG for type-I *vs*. type-II collagen. The histograms show that a strong discrimination between these collagen types can be achieved. 2-D images of these ratios for collagen-I dominated rail tail tendon (left column) *vs*. type-II dominated rat trachea (right column) shows consistent differences. Reproduced from Su *et al*. (36) with permission. SHG, second harmonic generation.

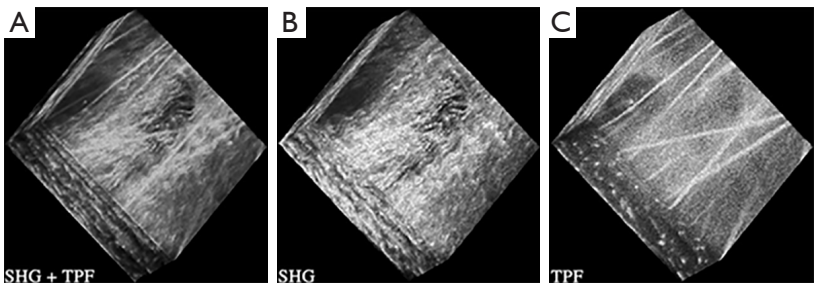

Figure 9 3-D stack of SHG and TPF emission from the superficial zone of bovine articular cartilage. The 800 nm excitation is too long to excited collagen autofluorescence and hence narrow-band 400 nm imaging isolates collagen SHG whereas imaging the Stokes-shifted radiation reveals a spatially uncorrelated fibrous component which is identified as elastin. This appears to be the first consistent report of the existence of elastic fibers in the superficial zone, which confirms the power of the multi-photon technique. Reproduced from Yeh *et al*. (32) with permission. SHG, second harmonic generation.

The search for additional contrast in SHG imaging has suggested the possibility of using the ratio of forward to backward generated signal intensities (39). SHG emission requires photon momentum conservation in addition to photon energy conservation and this is expressed as a phase-matching requirement between the excitation and emission electromagnetic waves. The degree of phase matching is strongly influenced by the microstructural properties of the material, especially by the phenomenon of quasi-phase matching (40). The degree of phase matching in turn influences the ratio of signal intensities generated in the forward and backward directions. For thick, turbid tissue samples these signals can be difficult to separate because intense elastic scatter of the emitted photons randomizes the emitted photon trajectories. Brown *et al*. therefore used 10 micron histological sections of human tibial plateau cartilage, both from normal patients (undergoing above-knee amputations) and from sufferers of antero-medial osteoarthritis, which is a type of osteoarthritis in which a full spectrum of cartilage degeneration can generally be found on the same joint. It was found that the forward/backward ratio was significantly enhanced in highly degenerated cartilage, relative to normal tissue (41). A Hertz-vector formalism was developed to theoretically relate the measurements to the tissue microstructure and this suggests that the enhanced forward signal relative to

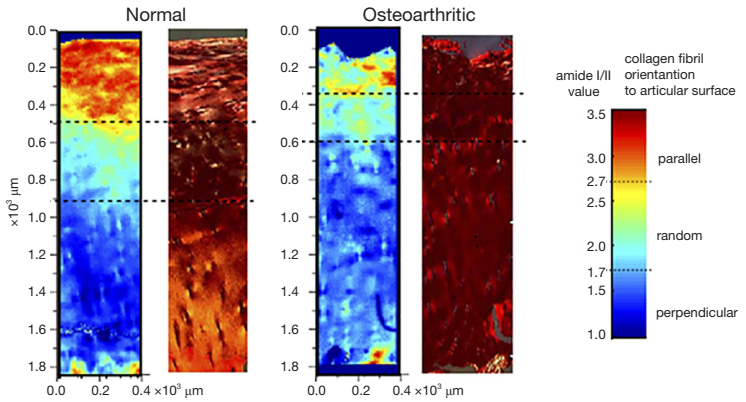

Figure 10 Polarized light FTIR imaging of the amide I/II band ratio correlated with conventional polarized light imaging. Left pair of images: normal cartilage. Right pair: osteoarthritic cartilage. The superficial, transitional and radial zones are clearly identified by PLM for normal cartilage and correlate closely with the amide I/II ratio as measured using IR light that is polarized in the direction of the surface normal. For osteoarthritic cartilage both techniques show a loss of organization throughout the cartilage depth. Reproduced from Bi *et al*. (44) with permission. FTIR, Fourier-transform infrared; PLM, polarized light microscopy.

backward signal is indicative of the formation of larger bundles of collagen fibrils in the diseased state.

Vibrational spectroscopy and imaging

The mid-IR spectrum contains much richer chemical composition information than the visible and near-infrared bands, due to the low energy molecular rotational/vibrational transitions in complex organic molecules. This part of the spectrum can be probed directly using Fourier transform infrared (FTIR) spectroscopy and spectral imaging. It can also be probed indirectly using spontaneous and coherent Raman techniques. The major advantage of the FTIR approach is the very wide spectral coverage coupled with short data acquisition times. The major advantage of spontaneous Raman is its much better penetration into water-rich tissues and the major advantage of coherent Raman techniques such as CARS and SRS is the much greater signal strength compared to spontaneous Raman whilst retaining good penetration into biological tissues and the intrinsic optical sectioning which facilitates high quality volumetric imaging (42).

An extremely useful feature of IR absorbance is the strong linear dichroism that is displayed by many of the vibrational transition dipole moments. Like birefringence, dichroism is mediated by the first-order susceptibility tensor $\chi^{(1)}$ and is due to the imaginary component of the refractive index being polarization-dependent. Camacho *et al.* studied 6 µm adult bovine occipital joints using linearly polarized IR light and noted how the intensity of the Amide-I and Amide-II bands varied with the polarization angle of the beam (43). In the superficial zone, it is found that the amide-II band falls relative to amide-I when the polarization angle moves from being parallel to the surface to being perpendicular to it. In the radial zone however this trend is reversed. The interpretation of this is that the amide-II transition dipole moment lies along the collagen fibril long axis and hence shows the greatest absorbance when the polarization direction is parallel to the fibril axis. The amide-I dipole moment however is generally thought to be oriented orthogonal to the fibril long-axis. By carefully calibrating this approach using type-I collagen from rabbit knee cartilage, Bi *et al*. refined these measurements into quantified maps of the collagen orientation in 7 µm slices of equine femoral condyle cartilage (normal and microfracture-repair tissue) and human tibial plateau cartilage (normal and osteoarthritic) (44). Maps showing the expected realignment, relative to the surface, from parallel to perpendicular were produced which correlate very well with contemporary polarized light micrographs taken with crossed polarizers in normal tissue (*Figure 10*). In microfracture repair tissue and osteoarthritic tissue, the fiber orientation was more disorganized and the strong zonal differentiation lost.

Lee and Xia recently emphasized the importance of correlating FTIR maps of zonal architecture against other methods such as PLM and magnetic resonance microscopy (45). Semi-empirical criteria were established for quantifying the zonal thicknesses from each modality

e.g., the most disordered zone of collagen (taken to represent the mid-point of the transitional zone) was associated with the minimum optical retardation in a PLM image, the depth where the depth-resolved Amide-I and Amide-II dichroic ratios (absorbance ratio for light polarized parallel and perpendicular to the articular surface respectively) cross over and finally the depth at which the MRI T2 relaxation time reaches a maximum, given a B-field aligned parallel with the articular surface. Good correlation was found between the measurements of transitional zone thickness by these three techniques (80±25, 71±25 and 83±19 microns respectively for averages across 18 sites taken from canine humeral cartilage samples).

FTIR is predominantly an *in vitro* technique at the moment, especially if high spatial resolution mapping is required. Raman spectroscopy avoids problems of intense water absorption and is better suited to reflectance mode imaging *in vivo*. A disadvantage is the weakness of the signal relative to e.g., fluorescence. However, there have been useful reports applying the technique to cartilage. Lim *et al.* used Raman spectroscopy using 1 mW of excitation power at 785 nm to obtain spectra from a 1 micron spot on the surface of porcine tibial cartilage (46). Explants were imaged before and after impact testing using a variety of impact pressures generated by a commercial impact tester. Samples were also assessed for cell viability using fluorescence confocal imaging of propidium iodide and were scored on the Mankin scale using H&E and Safranin-O/Fast Green staining. Polarized Raman spectroscopy demonstrated changes in 1,126 cm^{-1} band intensity (assigned to the pyranose ring structure and hence a marker for GAG concentration) as well as Amide III red shifts (interpreted as compression of the C-N bonds in collagen). Interestingly these changes appeared at all impact pressures 15, 20 and 25 MPa whereas cell viability and Mankin scoring detected changes only for 20 and 25 MPa, suggesting a potential role for Raman spectroscopy in detecting very early structural changes due to impact damage. Before leaving this point it is worth pointing out that polarized Raman band intensity, like linear birefringence and dichroism, is mediated by $\chi^{(1)}$ and thus similar geometrical considerations apply to the interpretation of polarized Raman spectra as applies to interpreting linear birefringence in a complex, zonal, 3-D fibrillar structure such as cartilage (see section Polarization-sensitive OCT). Galvis *et al.* studied the effect of the orientation in 3-D space of collagen bundles in rat tail tendon on the polarized Raman spectrum, in particular the Amide-I intensity at 1,600-1,700 cm^{-1} (47). Strong polarization sensitivity is shown when the fibril lies in the same plane as the incident E-field but this sensitivity is greatly reduced when the fibril is oriented parallel to the k-vector of the beam. This could form the basis of 3-D mapping of collagen orientation.

A distinct, but closely related, technique to Raman is Brillouin scattering microscopy. Both techniques excite a sample with an optical or NIR photon and detect inelastically Stokes shifted emission. In Raman scattering the frequency shift is imparted by molecular rotational and vibrational oscillations, which cause a periodic spatially localized oscillation in $\chi^{(1)}$. In Brillouin scattering the Stokes shift is caused by scattering off a thermally excited propagating acoustic wave, which causes temporal and spatial fluctuations in $\chi^{(1)}$ due to compression and rarefaction of the bulk medium. These spontaneously generated acoustic waves propagate at ~3,000 ms^{-1} and thus induce frequency shifts in the 10's of GHz range, which is detected by various methods, including high-finesse Fabry-Perot interferometers or optical beating (48). This technique has recently been applied to articular cartilage and extracellular matrix components such as collagen and elastin (49), demonstrating for example that the elastic moduli of collagen and elastin are much higher when measured at the scale of an individual fiber than when inferred from bulk mechanical testing at lower frequencies. This could indicate that molecular scale viscoelastic effects predominantly determine the frequency dependence of the mechanical properties of these materials. For equine metacarpophalangeal cartilage, increased stiffening and reduced acoustic damping correlated with increasing dehydration. Interestingly, directionally resolved measurement of acoustic wave speed showed no evidence of directional anisotropy, which can be contrasted with the very strong optical anisotropy exhibited by the tissue, as discussed in previous sections of this review.

Fluorescence and multispectral reflectance imaging

A class of techniques that have been relatively little used to date but which have excellent potential, particularly for low-cost clinical examination tools, are those that use optical and near-infrared diffuse light. Kinnunen *et al.* used visible wavelength multispectral imaging using a liquid crystal tunable filter to image the surface of normal bovine patellar cartilage and cartilage that had been degraded either enzymatically using collagenase or mechanically using abrasive paper (50). The reflectance spectrum of enzymatically

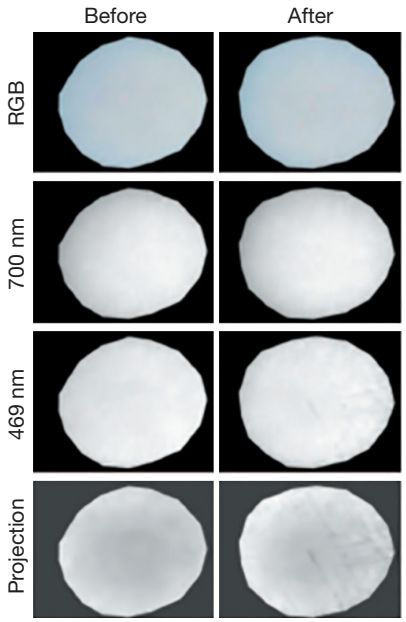

Figure 11 Multi-spectral images obtained from mechanically degraded articular cartilage. Top row: representation by projecting the spectral data onto an RGB color space. Second row: image in a narrow band at 700 nm. Third row: ditto at 469 nm. Bottom row: image of the data set projected onto the second principal component. There is enhanced contrast to the surface scratches produced by debriding with emery paper. Reproduced from Kinnunen *et al.* (50) with permission. RGB, red, green and blue.

degraded cartilage showed a clear trend towards that of haemoglobin and may reveal thinning of the cartilage layer and hence an increased signal contribution from the vascular network in the subchondral bone. Mechanical surface degradation (grinding tracks) could be visualized with enhanced contrast, relative to monochromatic imaging, by applying principal component analysis to the multispectral data sets (*Figure 11*). The eigenvector carrying spectral information from haemoglobin identified degradation that was invisible under 700 nm narrow-band imaging and with better contrast than 469 nm imaging.

The same group have also recently evaluated the utility of fluorescence imaging as a non-invasive tool to assess collagen cross-linking. It has been established by fluorescence microscopy of excised sections, that cartilage collagen displays a substantial autofluorescence background due primarily to the steady accumulation of advanced glycation products (AGE's) with increasing age (51). This background can be reduced in areas of strong matrix remodelling, e.g., in areas of osteoarthritic change. Kinnunen *et al.* used a wholly non-invasive fluorescence spectroscopy system to measure intact osteochondral cartilage plugs harvested from the bovine knee joint (52). Using an excitation monochromator and array spectrometer to collect an excitation/emission matrix, samples treated with the cross-linking promoter threose were compared with untreated control samples. It was found that increased cross-linking caused an increase in autofluorescence when longer excitation wavelengths were used but a decrease when shorter wavelengths were used, suggesting a change in the relative abundance of fluorescent species contributing to the overall signal from cartilage.

Conclusions

Optical and near-infrared imaging and spectroscopy are capable of providing unique data concerning the collagen architecture of articular cartilage. Whilst techniques such as FTIR and qPLM remain largely applicable only to *in vitro* studies, recent years have seen a rapid expansion in the availability of techniques that could potentially be used *in vivo*, thus providing tools that could allow the in-situ monitoring of 3-D collagen architecture during an arthroscopy examination. The improved detection of morphological alterations in collagen architecture could improve arthroscopically guided interventions such as debridement, monitor the success of regenerative treatments such as autologous chondrocyte implantation and potentially guide the fabrication of tissue engineering scaffolds.

Disclosure: The authors declare no conflict of interest.

References

1. Katta J, Jin Z, Ingham E, Fisher J. Biotribology of articular cartilage--a review of the recent advances. Med Eng Phys 2008;30:1349-63.
2. Hunziker EB. Articular cartilage repair: basic science and clinical progress. A review of the current status and prospects. Osteoarthritis Cartilage 2002;10:432-63.
3. Wolman M, Kasten FH. Polarized light microscopy in the study of the molecular structure of collagen and reticulin. Histochemistry 1986;85:41-9.
4. Benninghoff A. Form und Bau der Gelenkknorpel in ihren Beziehungen zur Funktion. II. Der Aufbau des Gelenkknorpels in seinen Beziehungen zur Funktion. Zeitschrift für Zellforschung and mikroskopische

Anatomie 1925;2:783-862.
5. Clark JM. The organisation of collagen fibrils in the superficial zones of articular cartilage. J Anat 1990;171:117-30.
6. Jeffery AK, Blunn GW, Archer CW, Bentley G. Three-dimensional collagen architecture in bovine articular cartilage. J Bone Joint Surg Br 1991;73:795-801.
7. Rieppo J, Hallikainen J, Jurvelin JS, Kiviranta I, Helminen HJ, Hyttinen MM. Practical considerations in the use of polarized light microscopy in the analysis of the collagen network in articular cartilage. Microsc Res Tech 2008;71:279-87.
8. Xia Y, Moody JB, Burton-Wurster N, Lust G. Quantitative in situ correlation between microscopic MRI and polarized light microscopy studies of articular cartilage. Osteoarthritis Cartilage 2001;9:393-406.
9. Mittelstaedt D, Xia Y, Shmelyov A, Casciani N, Bidthanapally A. Quantitative determination of morphological and territorial structures of articular cartilage from both perpendicular and parallel sections by polarized light microscopy. Connect Tissue Res 2011;52:512-22.
10. Rieppo J, Hyttinen MM, Halmesmaki E, Ruotsalainen H, Vasara A, Kiviranta I, Jurvelin JS, Helminen HJ. Changes in spatial collagen content and collagen network architecture in porcine articular cartilage during growth and maturation. Osteoarthritis Cartilage 2009;17:448-55.
11. Wilson W, van Donkelaar CC, van Rietbergen B, Ito K, Huiskes R. Stresses in the local collagen network of articular cartilage: a poroviscoelastic fibril-reinforced finite element study. J Biomech 2004;37:357-66.
12. Julkunen P, Kiviranta P, Wilson W, Jurvelin JS, Korhonen RK. Characterization of articular cartilage by combining microscopic analysis with a fibril-reinforced finite-element model. J Biomech 2007;40:1862-70.
13. Nissi MJ, Rieppo J, Töyräs J, Laasanen MS, Kiviranta I, Jurvelin JS, Nieminen MT. T(2) relaxation time mapping reveals age- and species-related diversity of collagen network architecture in articular cartilage. Osteoarthritis Cartilage 2006;14:1265-71.
14. Herrmann JM, Pitris C, Bouma BE, Boppart SA, Jesser CA, Stamper DL, Fujimoto JG, Brezinski ME. High resolution imaging of normal and osteoarthritic cartilage with optical coherence tomography. J Rheumatol 1999;26:627-35.
15. Chu CR, Lin D, Geisler JL, Chu CT, Fu FH, Pan Y. Arthroscopic microscopy of articular cartilage using optical coherence tomography. Am J Sports Med 2004;32:699-709.
16. Cernohorsky P, de Bruin DM, van Herk M, Bras J, Faber DJ, Strackee SD, van Leeuwen TG. In-situ imaging of articular cartilage of the first carpometacarpal joint using co-registered optical coherence tomography and computed tomography. J Biomed Opt 2012;17:060501.
17. te Moller NC, Brommer H, Liukkonen J, Virén T, Timonen M, Puhakka PH, Jurvelin JS, van Weeren PR, Töyräs J. Arthroscopic optical coherence tomography provides detailed information on articular cartilage lesions in horses. Vet J 2013;197:589-95.
18. Patel NA, Zoeller J, Stamper DL, Fujimoto JG, Brezinski ME. Monitoring osteoarthritis in the rat model using optical coherence tomography. IEEE Trans Med Imaging. 2005;24:155-9.
19. Schmitt JM, Knüttel A, Bonner RF. Measurement of optical properties of biological tissues by low-coherence reflectometry. Appl Opt 1993;32:6032-42.
20. Bear DM, Szczodry M, Kramer S, Coyle CH, Smolinski P, Chu CR. Optical coherence tomography detection of subclinical traumatic cartilage injury. J Orthop Trauma 2010;24:577-82.
21. Shyu JJ, Chan CH, Hsiung MW, Yang PN, Chen HW, Kuo WC. Diagnosis of articular cartilage damage by polarization sensitive optical coherence tomography and the extracted optical properties. Progress In Electromagnetics Research 2009;91:365-76.
22. Thrane L, Yura HT, Andersen PE. Analysis of optical coherence tomography systems based on the extended Huygens-Fresnel principle. J Opt Soc Am A Opt Image Sci Vis 2000;17:484-90.
23. de Boer JF, Milner TE. Review of polarization sensitive optical coherence tomography and Stokes vector determination. J Biomed Opt 2002;7:359-71.
24. Li X, Martin S, Pitris C, Ghanta R, Stamper DL, Harman M, Fujimoto JG, Brezinski ME. High-resolution optical coherence tomographic imaging of osteoarthritic cartilage during open knee surgery. Arthritis Res Ther 2005;7:R318-23.
25. Chu CR, Izzo NJ, Irrgang JJ, Ferretti M, Studer RK. Clinical diagnosis of potentially treatable early articular cartilage degeneration using optical coherence tomography. J Biomed Opt 2007;12:051703.
26. Ugryumova N, Gangnus SV, Matcher SJ. Three-dimensional optic axis determination using variable-incidence-angle polarization-optical coherence tomography. Opt Lett 2006;31:2305-7.
27. Ugryumova N, Jacobs J, Bonesi M, Matcher SJ. Novel

optical imaging technique to determine the 3-D orientation of collagen fibers in cartilage: variable-incidence angle polarization-sensitive optical coherence tomography. Osteoarthritis Cartilage 2009;17:33-42.
28. Kasaragod DK, Lu Z, Jacobs J, Matcher SJ. Experimental validation of an extended Jones matrix calculus model to study the 3D structural orientation of the collagen fibers in articular cartilage using polarization-sensitive optical coherence tomography. Biomed Opt Express 2012;3:378-87.
29. Lu Z, Kasaragod D, Matcher SJ. Conical scan polarization-sensitive optical coherence tomography. Biomed Opt Express 2014;5:752-62.
30. Ugryumova N, Attenburrow DP, Winlove CP, Matcher SJ. The collagen structure of equine articular cartilage, characterized using polarization-sensitive optical coherence tomography. J Phys D: Appl Phys 2005;38:2612-19.
31. Xie T, Guo S, Zhang J, Chen Z, Peavy GM. Use of polarization-sensitive optical coherence tomography to determine the directional polarization sensitivity of articular cartilage and meniscus. J Biomed Opt 2006;11:064001.
32. Yeh AT, Hammer-Wilson MJ, Van Sickle DC, Benton HP, Zoumi A, Tromberg BJ, Peavy GM. Nonlinear optical microscopy of articular cartilage. Osteoarthritis Cartilage 2005;13:345-52.
33. Mansfield JC, Winlove CP, Moger J, Matcher SJ. Collagen fiber arrangement in normal and diseased cartilage studied by polarization sensitive nonlinear microscopy. J Biomed Opt 2008;13:044020.
34. Fu L, Jain A, Xie H, Cranfield C, Gu M. Nonlinear optical endoscopy based on a double-clad photonic crystal fiber and a MEMS mirror. Opt Express 2006;14:1027-32.
35. Freund I, Deutsch M, Sprecher A. Connective tissue polarity. Optical second-harmonic microscopy, crossed-beam summation, and small-angle scattering in rat-tail tendon. Biophys J 1986;50:693-712.
36. Su PJ, Chen WL, Li TH, Chou CK, Chen TH, Ho YY, Huang CH, Chang SJ, Huang YY, Lee HS, Dong CY. The discrimination of type I and type II collagen and the label-free imaging of engineered cartilage tissue. Biomaterials 2010;31:9415-21.
37. Yu J, Urban JP. The elastic network of articular cartilage: an immunohistochemical study of elastin fibres and microfibrils. J Anat 2010;216:533-41.
38. Bell JS, Christmas J, Mansfield JC, Everson RM, Winlove CP. Micromechanical response of articular cartilage to tensile load measured using nonlinear microscopy. Acta Biomater 2014;10:2574-81.
39. Campagnola P. Second harmonic generation imaging microscopy: applications to diseases diagnostics. Anal Chem 2011;83:3224-31.
40. Lacomb R, Nadiarnykh O, Townsend SS, Campagnola PJ. Phase Matching considerations in Second Harmonic Generation from tissues: Effects on emission directionality, conversion efficiency and observed morphology. Opt Commun 2008;281:1823-1832.
41. Brown CP, Houle MA, Popov K, Nicklaus M, Couture CA, Laliberté M, Brabec T, Ruediger A, Carr AJ, Price AJ, Gill HS, Ramunno L, Légaré F. Imaging and modeling collagen architecture from the nano to micro scale. Biomed Opt Express 2013;5:233-43.
42. Mansfield JC, Winlove CP. A multi-modal multiphoton investigation of microstructure in the deep zone and calcified cartilage. J Anat 2012;220:405-16.
43. Camacho NP, West P, Torzilli PA, Mendelsohn R. FTIR microscopic imaging of collagen and proteoglycan in bovine cartilage. Biopolymers 2001;62:1-8.
44. Bi X, Li G, Doty SB, Camacho NP. A novel method for determination of collagen orientation in cartilage by Fourier transform infrared imaging spectroscopy (FT-IRIS). Osteoarthritis Cartilage 2005;13:1050-8.
45. Lee JH, Xia Y. Quantitative zonal differentiation of articular cartilage by microscopic magnetic resonance imaging, polarized light microscopy, and Fourier-transform infrared imaging. Microsc Res Tech 2013;76:625-32.
46. Lim NS, Hamed Z, Yeow CH, Chan C, Huang Z. Early detection of biomolecular changes in disrupted porcine cartilage using polarized Raman spectroscopy. J Biomed Opt 2011;16:017003.
47. Galvis L, Dunlop JW, Duda G, Fratzl P, Masic A. Polarized Raman anisotropic response of collagen in tendon: towards 3D orientation mapping of collagen in tissues. PLoS One 2013;8:e63518.
48. Scarcelli G, Yun SH. Confocal Brillouin microscopy for three-dimensional mechanical imaging. Nat Photonics 2007;2:39-43.
49. Palombo F, Winlove CP, Edginton RS, Green E, Stone N, Caponi S, Madami M, Fioretto D. Biomechanics of fibrous proteins of the extracellular matrix studied by Brillouin scattering. J R Soc Interface 2014;11:20140739.
50. Kinnunen J, Jurvelin JS, Mäkitalo J, Hauta-Kasari M, Vahimaa P, Saarakkala S. Optical spectral imaging of degeneration of articular cartilage. J Biomed Opt 2010;15:046024.
51. Gibson GJ, Verner JJ, Nelson FR, Lin DL. Degradation of the cartilage collagen matrix associated with changes

in chondrocytes in osteoarthrosis. Assessment by loss of background fluorescence and immunodetection of matrix components. J Orthop Res 2001;19:33-42.
52. Kinnunen J, Kokkonen HT, Kovanen V, Hauta-Kasari M, Vahimaa P, Lammi MJ, Töyräs J, Jurvelin JS. Nondestructive fluorescence-based quantification of threose-induced collagen cross-linking in bovine articular cartilage. J Biomed Opt 2012;17:97003.

Cite this article as: Matcher SJ. What can biophotonics tell us about the 3D microstructure of articular cartilage? Quant Imaging Med Surg 2015;5(1):143-158. doi: 10.3978/j.issn.2223-4292.2014.12.03

